PAPER

Enhanced activity of desilicated Cu-SSZ-13 for the selective catalytic reduction of NO$_x$ and its comparison with steamed Cu-SSZ-13†

R. Oord, [iD] I. C. ten Have, J. M. Arends, F. C. Hendriks, J. Schmidt, I. Lezcano-Gonzalez and B. M. Weckhuysen [iD] *

Mesoporous Cu-SSZ-13 was created by first synthesizing zeolite H-SSZ-13 and subsequently desilicating the material by base leaching using NaOH in different concentrations. The catalyst materials were prepared by ion exchanging the leached samples back to their acidic form using NH$_4$NO$_3$, and to their active Cu form by ion exchanging them with CuSO$_4$. For comparison, H- and Cu-SSZ-13 were steamed using a wide variety of different conditions. Using a 0.10 M NaOH solution for base leaching, it was found that Cu-SSZ-13 becomes more active in the selective catalytic reduction of NO$_x$ with NH$_3$ (NH$_3$-SCR) over the entire temperature region but especially in the low temperature region (<200 °C). This increase could be explained by a decrease in pore diffusion limitations due to the introduction of mesopores on the outside of the zeolite crystals but keeping the chemical environment of the catalyst nearly the same as that of the parent material. Higher base leaching concentrations do, however, lead to a decrease in the amount of Brønsted acid sites, pore volume and accessible surface area, accompanied by a decrease in NH$_3$-SCR activity. Ar physisorption coupled with SEM and confocal fluorescence microscopy in combination with two differently sized fluorescent organic probe molecules (*i.e.*, 4-(4-dimethyl-aminostyryl)-1-methyl-pyridinium-iodide and 4-(4-dicyclohexyl-aminostyryl)-1-methyl-pyridinium-iodide) show an increase in the external surface area due to the creation of mesopores. The development of mesoporosity starts from the crystal surface and continues into the crystal with increasing alkaline solution strength, but under our conditions it never reaches the center. On the other hand, zeolite steaming did not successfully introduce mesoporosity and mainly managed to deactivate the Cu-SSZ-13 zeolite catalysts.

Introduction

NH$_3$ Selective Catalytic Reduction (NH$_3$-SCR) of nitrogen oxides (NO$_x$) is an important technology to reduce environmentally harmful NO$_x$ from exhaust gases originating from mobile sources, such as cars, trucks and ships.[1] As environmental laws are becoming stricter, further development of NH$_3$-SCR technology and understanding of the catalyst materials employed are becoming more and more important. A very promising technique is NH$_3$-SCR using Cu- or Fe-exchanged zeolites. Amongst them, Cu-exchanged SSZ-13 zeolites have proven to be particularly active and selective in NH$_3$-SCR catalysis over a wide temperature window.[2–10] SSZ-13 is a zeolite with the chabazite (CHA) framework structure containing small radius (~3.8 Å) eight-membered ring pores (8 MR), as opposed to earlier NH$_3$-SCR investigated Cu-zeolite systems, such as Cu-ZSM-5 (10 MR; ~5.5 Å) and Cu-MOR (12 MR; ~6.5 Å).[8,11] These small pores are most likely the reason why catalyst materials, such as Cu-SSZ-13 and Cu-SAPO-34, are so active in the NH$_3$-SCR reaction. On the other hand, their small pore system may also cause problems, like diffusion limitations, thereby limiting the physical transport of reactants to the active sites.[12] For instance, Peden and co-workers have found that pore diffusion limitations play a significant role in the low-temperature kinetics of the zeolite Cu-SSZ-13 catalyst.[13] Extensive research to reveal the active site under operation and to obtain a consistent reaction mechanism has been performed in a collaborative manner by the groups of Beato, Lamberti and Bordiga,[14–18] as well as by the groups of Ribeiro and Schneider.[19–21] For example, Lomachenko *et al.* have shown that low temperature NH$_3$-SCR (up to 200 °C) is also characterized by balanced populations of Cu(I)/Cu(II) sites and mostly dominated by NH$_3$-solvated mobile species. Ribeiro, Schneider and co-workers have shown that for isolated Cu species, there can be different exchange positions, and that they are dependent on the conditions under which they are

Inorganic Chemistry and Catalysis, Debye Institute for Nanomaterials Science, Utrecht University, Universiteitsweg 99, 3584 CG, Utrecht, The Netherlands. E-mail: B.M.Weckhuysen@uu.nl

This journal is © The Royal Society of Chemistry 2017

Catal. Sci. Technol., 2017, **7**, 3851–3862 | 3851

measured; at low loadings, they will mainly occupy the 6 MR, first on 6 MR with 2 Al atoms, and later also on single Al sites, and both are hydrated easily at low temperatures by either water or NH_3.[19–21] Beato, Lamberti, Bordiga and co-workers also showed the effects of dehydration of Cu species inside the SSZ-13 framework and presented a consistent reaction scheme for NH_3-SCR. The SCR reaction can, according to them, be divided into oxidation of the catalyst by NO + O_2 and reduction by NO + NH_3. Furthermore, both NO and NH_3 are required in the reduction, and finally, oxidation by NO + O_2 or NO_2 leads to the same state of the catalyst.[14–18]

Mesopores inside the framework could improve the diffusion inside the zeolite.[22–24] Zhang *et al.* also performed some desilication experiments on SSZ-13 and modified this mesoporous zeolite with a mesoporous silica layer covering the outer surface.[23] They showed that by using this outer layer, the zeolite was better protected during hydrothermal aging.

Mesopores in zeolites can be formed either by post-synthesis methods or during synthesis. Post-treatment methods include steaming for dealumination and base leaching by breaking Si–O–Si and Si–O–Al bonds for desilication.[12] It was found that desilication using base leaching selectively removes silicon from the framework, leaving the Al sites, which are needed for Cu-ion exchange sites, unaltered.[12,23] For H-SSZ-13, this has been carried out by Sommer *et al.*[25] but using methanol-to-olefins (MTO) as the reaction of interest, in which the authors did not observe an enhancement of the catalytic properties of H-SSZ-13.[25] A key factor to optimize these treatments seems to be the concentration of the applied alkaline solution, and for this zeolite topology and slightly different Si/Al ratio this method still has to be optimized.

In this paper, we study the effect of base leaching on zeolite H-SSZ-13, subsequently followed by Cu ion exchange to obtain Cu-SSZ-13 materials. For comparison, steamed H- and Cu-SSZ-13 zeolite materials were also investigated. Both sets of catalyst materials, prepared by desilication or steaming, have been characterized by X-ray diffraction (XRD), scanning electron microscopy (SEM), UV-vis-NIR diffuse reflectance spectroscopy (DRS), temperature programmed desorption (TPD) of NH_3, Ar physisorption and confocal fluorescence microscopy in combination with two differently sized fluorescent organic probe molecules, *i.e.*, 4-(4-dimethylaminostyryl)-1-methyl-pyridinium-iodide and 4-(4-dicyclohexylaminostyryl)-1-methyl-pyridinium-iodide. The zeolites have been tested as catalysts in the $deNO_x$ NH_3-SCR reaction. It is known that the introduction of mesopores into microporous zeolite materials can lead to improved catalytic performance as a result of enhanced diffusion of both reactants and products,[24] especially in the low temperature regime where Cu-SSZ-13 is known to be not very effective in NH_3-SCR. Here, we show that by using a 0.10 M NaOH solution for base leaching, Cu-SSZ-13 becomes more active over the entire temperature region but especially below 200 °C. This increase could be explained by a decrease in the pore diffusion limitations due to the introduction of mesopores on the outer faces of the zeolite but

keeping the chemical environment of the catalyst the same as that of the parent material. Steaming, however, leads to catalyst deactivation and is shown to not produce any large mesopores in this zeolite system.

Experimental

Catalyst synthesis

25 wt% solution of a structure directing agent (SDA, *N,N,N*-trimethyl-1-adamantammonium) (Sachem, pure) was added to tetra-ethyl orthosilicate (TEOS, Aldrich, >99%) and aluminium isopropoxide (Acros Organics, 98%+). The resulting mixture was aged at RT for ~4 days. After this a 51% HF solution (Acros organics, 48–51%) was added and stirred to a homogeneous gel. The gel was transferred into three Teflon lined autoclaves, in equal portions. The autoclaves were sealed and put in a static oven at 150 °C for 6 days. After the synthesis was finished, the resulting solid was washed thoroughly (~8 L) with demineralized water. The resulting solid was a white powder. The SDA was burned away during calcination. The calcination was performed in a static oven at 580 °C for 3 h. Crystallinity was evaluated with XRD. The method used was adapted from Lezcano-Gonzalez *et al.*[26]

Alkaline treatment was carried out at 75 °C for 2 h using 20 mL solution per gram H-SSZ-13. The treatment was executed with a 0.10, 0.15, 0.20 M and 0.30 M sodium hydroxide (Merck, EMSURE, ISO) solution (Milli-Q H_2O). After the alkaline treatment, the sample was thoroughly washed with deionized water until neutral pH and dried overnight at 60 °C. To regain the protonated zeolite, three-fold ion exchange with 1.0 M NH_4NO_3 (Sigma Aldrich, 99.0%) (20 mL g^{-1}) was performed for 2 h at 75 °C to restore acidity. The sample was then washed with deionized water, followed by another calcination at 550 °C for 2 h in air, using a ramp of 5 °C min^{-1}. The Cu ion exchange was performed using 1 g SSZ-13 with 50 mL of 0.1 M $CuSO_4·5H_2O$ (pH = 4.3) (Merck ACS, ISO, Reag. Ph Eur) solution at 80 °C for 2 h. The resulting Cu-SSZ-13 material was washed with demineralized water and dried at 60 °C overnight. Calcination of the Cu-SSZ-13 material was performed at 550 °C for 4 h in a static oven in air.

The synthesis of 4-(4-dimethylaminostyryl)-1-methyl-pyridinium-iodide and 4-(4-dicyclohexylaminostyryl)-1-methyl-pyridinium-iodide is described in a recent paper from our group, and these probe molecules have been abbreviated as DAMPI-1 and DAMPI-4, respectively.[27]

Steaming was performed in a quartz reactor containing 1.0 gram of either Cu-SSZ-13 or H-SSZ-13, making use of 200 ml min^{-1} N_2 and a total of ~80%$_v$ steam. Two steaming conditions were used; mild and severe. The mild steaming conditions were as follows: *i.e.*, 2 °C min^{-1} to 350 °C, dwell at 350 °C for 30 min, and then increase with 1 °C min^{-1} towards 500 or 650 °C, and dwell at that final temperature for 5 h. When 350 °C was reached, steam was added to the flow. The steam was stopped before cooling down. Instead, severe steaming conditions were applied as follows: *i.e.*, in 200 min the temperature was increased from RT to 350 °C, dwell at

that temperature for 60 min and in 100 min the temperature was further increased to 500 °C and dwell there for 30 min. In 150 min the temperature was increased to 650 or 750 °C, and that temperature was maintained for 13 h. The steam was added when the temperature reached 500 °C and stopped before cooling down. This procedure was adapted from ref. 28. The influence of the water content in the flow during steaming was also studied using a flow of 300 ml N_2 min^{-1}. The temperature was raised from RT to 150 °C in 2 h and 10 min, and this temperature was maintained for 30 min; then it was raised to 550 °C in 2 h and 30 min and kept at this temperature for 6 h. At 550 °C the water content in the gas feed stream was set at 15%, 40%, or 90%. Typically, 0.75 g of the sample was set on a semipermeable holder inside the quartz tube. As a result, a wide range of H-SSZ-13 and Cu-SSZ-13 samples have been created through steam treatment, which can be divided into 5 different sets. Table 1 summarizes the different materials prepared, together with their sample codes.

Catalyst characterization

The X-ray diffraction (XRD) patterns of the as-synthesized, calcined and Cu-exchanged samples were recorded on a Bruker D8 X-ray powder diffractometer equipped with a Co K_α X-ray tube ($\lambda = 1.7902$ Å). This Co K_α radiation has a different wavelength from the usually employed Cu K_α radiation in XRD equipment; hence the diffraction peaks will appear at different 2θ values.

UV-vis-NIR diffuse reflectance spectroscopy (DRS) was conducted using a Varian Cary 500 UV-vis-NIR spectrometer equipped with a DRS accessory to allow collection in diffuse reflectance mode against a pure white reference standard. Spectra were collected between 4000–50 000 cm^{-1} with a data interval of 10 cm^{-1} and at a rate of 6000 cm^{-1} min^{-1}. The UV-vis-NIR DRS spectra were corrected for the detector/grating and light source changeover steps at 11 400 + 12 500 cm^{-1} and 28 570 cm^{-1}, respectively.

Temperature programmed desorption of ammonia (NH_3-TPD) was performed using a Micromeritics ASAP-2020 equipped with a TCD detector. Prior to TPD, 0.1 g of catalyst was first outgassed in He for 1 h at 600 °C with a heating ramp of 10 °C min^{-1}. Ammonia was adsorbed at 100 °C until saturation, followed by flushing with He for 120 min at 100 °C. The ammonia desorption was monitored using the TCD detector until 700 °C with a ramp of 5 °C min^{-1}, using a flow of 25 mL min^{-1}.

Inductively coupled plasma optical emission spectrometry (ICP-OES) was carried out by the Geolab (Utrecht University) using a SPECTRO CIROS CCD instrument from SPECTRO Analytical Instruments. Samples were dissolved using an aqua regia with HF solution, in which they were dissolved at 90 °C overnight; after which the solution was cooled down to RT and neutralized using boric acid. After this the solutions were diluted to yield the appropriate concentrations.

N_2 adsorption–desorption isotherms were measured at −196 °C with a Micromeritics ASAP-2420 instrument. The Brunauer–Emmett–Teller (BET) method was utilized to calculate the specific surface areas of the solid catalyst particles, and the micropore volumes were calculated by using the t-plot approach. The samples were outgassed for 16 h at 350 °C under vacuum using a turbo molecular pump. Ar physisorption of the catalysts was performed with a Micromeritics TriStar 3000 instrument. Before the measurements, the samples were outgassed for 16 h at 380 °C under vacuum. Measurements were performed using Ar at −196 °C. The external surface area, micropore surface area and micropore volume were determined by applying the t-plot method.

Scanning electron microscopy (SEM) measurements were performed using an FEI XL30SFEG instrument. Prior to analysis, the zeolite crystals were coated with a ∼9 nm layer of Pt to increase the conductivity of the samples.

A Nikon Eclipse 90i microscope with a 100 × 0.73 NA dry objective was used for the confocal fluorescence microscopy investigations. The excitation light was a 488 nm laser. The microscope was equipped with a Nikon A1 scan head, accommodating the optics, which couple fiber optics for excitation and emission light with the microscope. A spectral analyzer in the Nikon A1 system was equipped with 32 photomultiplier tubes (PMTs) set to collect emission light in the region of 520–706 nm, with a resolution of 6 nm. Prior to the measurements, each sample was stained with either of the probe molecules DAMPI-1 or DAMPI-4 for one month. The excess probe molecule was washed from the surface of the zeolite using ethanol twice, after which the crystals were dried on a glass slide. The absorption maximum for DAMPI-1 lies at ∼481 nm and the cylinder-like molecule has an effective diameter of 5.8 Å,[27] which will not fit into the small 8-MR rings of SSZ-13, unless larger pores are created e.g. by NaOH leaching or steaming. On the other hand, DAMPI-4 with a

Table 1 Overview of the H-SSZ-13 and Cu-SSZ-13 samples prepared after steaming using a wide variety of conditions, including their sample codes

Parent material	Steaming program	Temperature (°C)	Duration (h)	Water content (%$_v$)	Sample code
H-SSZ-13	Mild	500, 650	5	80	m500, m650
H-SSZ-13	Severe	500, 650, 750	13	80	s500, s650, s750
Cu-SSZ-13	Mild	500, 650	5	80	m500, m650
Cu-SSZ-13	Severe	500, 650, 750	13	80	s500, s650, s750
Cu-SSZ-13	Mild[a]	550	6	15, 40, 90	15%, 40%, 90%

[a] Varying water content used, with a slightly different steaming program as compared to the mild program.

bulkier head having an effective diameter of 10.1 Å, cannot even fit in larger micropores created by *e.g.* steam treatment. Similar probes have been used to stain zeolite materials before[29–31] and have been specifically synthesized for use in these kinds of selective staining experiments.

Catalyst testing

Catalytic tests were performed in a fixed bed plug flow set-up. Typically, 50 mg of powdered catalyst material with sieve fractions of 0.425–0.150 mm was loaded in a 1 cm OD quartz tubular reactor. Prior to the experiment, the zeolite sample was pre-treated for 1 h with 5% O_2 in He at 550 °C. After the pre-treatment, the desired reaction temperature was fixed, and then the catalyst was exposed to a SCR feed composition of 1000 ppm NO, 1000 ppm NH_3 and 5% O_2, and He for balance, with a gas hourly space velocity (GHSV) of $100\,000\ h^{-1}$. Steady-state measurements were performed at different reaction temperatures, from 150 to 450 °C, using a stabilization period of 60 min at each temperature and the output gases were analyzed by mass spectrometry (Hiden Analytical, HPR-20 QIC) and FT-IR gas analysis. All SCR gases were provided by Linde. To avoid condensation in the reaction system, all the gas lines were heated to 150 °C.

The following formulas were used to calculate the NO conversion and N_2 selectivity, respectively:

$$\text{NO conversion}\,(\%) = \frac{NO_{in} - NO_{out}}{NO_{in}} \times 100$$

$$N_2\ \text{selectivity} = \frac{NO_{in} - NO_{out} - N_2O_{out} - NO_{2\,out}}{NO_{in}} \times 100$$

The following formulas were used to calculate the Thiele modulus and effectiveness factor for the zeolite particles under study. The necessary data were published by Gao *et al.*[13] For these measurements, we assume that the kinetic model also holds for the catalyst materials described in this work. The Thiele modulus can then be estimated by recalculating the effectiveness factor for 8 μm-sized samples (*i.e.*, a radius of 4 μm): $\varphi_1 = 15.1$ (IE 90%); $\varphi_2 = 4\,X$, $\varphi_1 = 60.24$; $\eta_2 = 3/(60.24)^2 \times (60.24\coth(60.24) - 1)$, $\eta_2 = 0.049$. The latter value indicates that only 5% of the zeolite catalyst material under study is used, so this is a very thin layer.

Results and discussion

Catalyst crystallinity and morphology

The X-ray diffraction (XRD) patterns of the parent H-SSZ-13 and base-leached Cu-SSZ-13 catalysts are shown in Fig. 1. It can be noted that the parent zeolite material exhibits all the characteristic diffraction peaks of the CHA framework. The characteristic CHA reflections decrease in intensity after treating the samples with NaOH, indicating that the zeolite crystals lose their crystallinity upon increasing the base concentration. Interestingly, at 0.2 M NaOH most of the zeolite
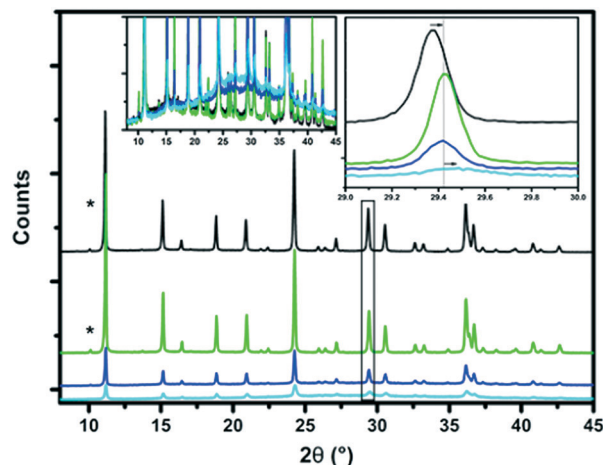

Fig. 1 XRD patterns of parent and base-leached zeolite H-SSZ-13. H-parent (black), 0.10 (green), 0.15 (dark blue) and 0.20 (cyan) peaks denoted * are due to k_β radiation. The right inset shows a zoomed-in view of one of the framework peaks at around 29° 2θ, while the left inset shows a zoomed-in view of the amorphous phase peaks.

crystallinity was lost. A new amorphous phase is detected at 2θ values around 28°, which is another indication that part of the zeolite framework is destroyed upon base leaching. From the zoomed-in view, we see a shift of the peak towards higher 2θ values, suggesting a lattice contraction as a result of a change in the chemical composition (removal of Si) of the unit cell of SSZ-13. ICP-OES revealed a decrease in the Si/Al ratio for the base-leached samples, as can be seen in Table 2. The combined results of these two methods indicate that it is silicon that is selectively removed from the zeolite framework by alkaline treatment and not aluminum, although at high NaOH concentrations this does lead to structural collapse. In addition, the Cu weight loading is not significantly different for the various base-leached zeolite H-SSZ-13 samples.

Fig. 2 shows the Ar physisorption isotherms and derived pore size distributions for the parent and base-leached Cu-SSZ-13 samples. For the fresh H-SSZ-13 and Cu-SSZ-13 samples, the isotherms show a type I isotherm, while for the base-leached samples the isotherms show a type IV hysteresis loop, indicative of mesoporosity. With increasing NaOH concentration, the hysteresis loop becomes more evident. However, in line with the findings reported by Sommer *et al.*, a decrease in BET surface area is observed with increasing NaOH concentration (Table 3).[25] However, we do see some differences compared to the observations of Sommer *et al.*[25] These authors reported an increase in the total pore volume, while we see a decrease in the total pore volume in this work.

An increase in the external pore volume was, however, observed with increasing NaOH concentration. This is logical since the external surface area also accounts for the mesopores. The micropore volume decreased from 0.26 to 0.04 mL g^{-1}, while the total pore volume decreased slightly from 0.28 to 0.18 mL. This means that the zeolite structure partially collapses and some of the micropores are therefore mostly blocked.

3854 | *Catal. Sci. Technol.*, 2017, **7**, 3851–3862

This journal is © The Royal Society of Chemistry 2017

Table 2 Si/Al and Cu/Al ratios of parent and base-leached Cu-SSZ-13 samples, as measured by ICP-OES and total NH_3 desorption per gram of zeolite

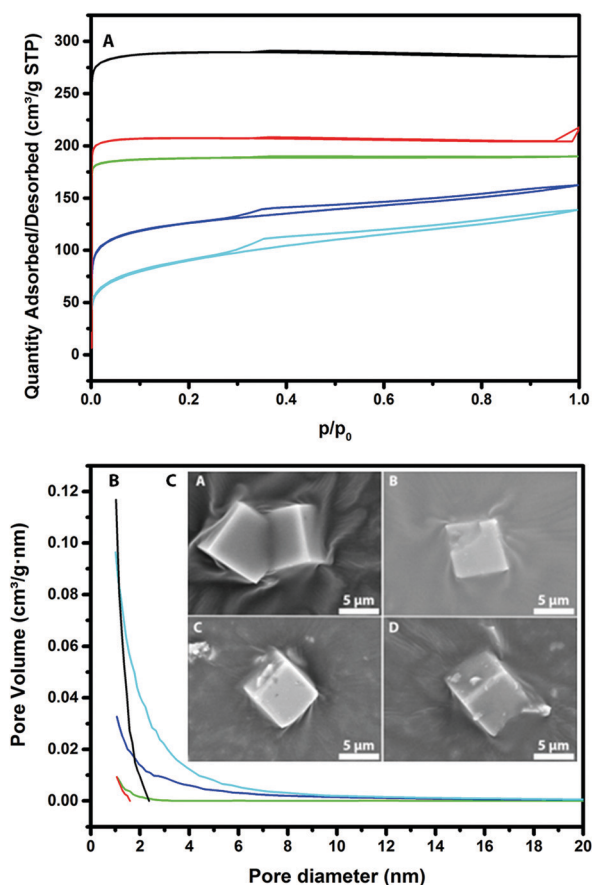| Sample	Si/Al ratio	Cu/Al ratio	Cu ($\%_{wt}$)	Quantity NH_3 adsorbed (cm^3 g^{-1} STP)[a]
H-Parent	17.8	—	—	21.0
Cu-Parent	17.6	0.68	1.3	21.7
#0.10	18.1	0.58	1.1	20.7
#0.15	15.1	0.52	1.1	17.6
#0.20	14.4	0.47	1.0	11.7

[a] As determined with NH_3-TPD.

The increase in mesopore volume is not enough to compensate for this loss in pore volume, so the net result is a small decrease in overall pore volume. Using the BJH method, a pore size distribution was generated, showing that the pores are about 1–3 nm in size, with a maximum of about

Fig. 2 Ar isotherms (A) and BJH size distributions (B) as calculated from the adsorption of Ar for H-parent (black), Cu-parent (red), 0.10 (green), 0.15 (dark blue) and 0.20 (cyan). (C) SEM images of the different zeolite materials under study, all at 12 000× magnification. A) H-SSZ-parent, B) Cu-SSZ-13-0.10, C) Cu-SSZ-13-0.15 and D) Cu-SSZ-13-0.20. Note that the samples might be a bit blurry or show low contrast. This is because we had to decrease the acceleration voltage (from 12 keV to 10 keV); otherwise, the crystals would crack instantaneously.

10 nm for the 0.2 M leached Cu-SSZ-13 sample. This differs a bit from the literature, where there is a broader distribution of mesopores reported for SSZ-13 materials.[25] To visualize how the zeolite crystals look before and after base leaching, scanning electron microscopy (SEM) images were recorded, as shown in Fig. 2. Using increasingly higher base concentrations, the surface of the zeolite crystal looks already a bit rougher than that of the parent material. A few "chips" of zeolite can also been seen on the surface, but this is probably due to sample preparation for the SEM measurements.

For comparison, the X-ray diffraction (XRD) patterns of the as-synthesized parent and steamed H-SSZ-13 and Cu-SSZ-13 catalyst materials are shown in Fig. S1.† The as-synthesized zeolite materials exhibit all the characteristic diffraction peaks of the CHA framework. Upon extensive aging, the Cu-SSZ-13-S750 material shows a decrease in crystallinity and the creation of an amorphous phase, as evidenced by the rise in background at around 28° 2θ and a severe decrease in all peak intensities (Fig. S1F†). For all catalyst materials treated in steam at temperatures <750 °C, no amorphous phase could be detected by XRD. A small shift in 2θ can be seen toward higher 2θ values; a close-up of this can be found in the inserts of Fig. S1.† This could be due to two reasons; (I) sample displacement or (II) a decrease in the unit cell size due to the removal of aluminum. For the H-SSZ-13 samples, the trend seems to be a decrease of the unit cell size with increasing steaming temperature. For the Cu-SSZ-13 samples, this cannot be concluded, since there is no clear trend observed (Fig. S1C and D†). Since the intensity of all crystal reflections remains stable, we can conclude that the CHA framework only collapses at temperatures >750 °C. The Cu-S750 sample shows a big loss in peak intensities, combined with a detectable amorphous phase at around 20–30° 2θ, indicating major degradation of the zeolite framework (Fig. S1F†). While investigating the influence of water content at 550 °C, no changes in XRD patterns were observed, as can be deduced from Fig. S1E.†

Furthermore, the BET surface areas and micropore volumes of the hydrothermally treated zeolite samples at $80\%_v$ water content, which were estimated from N_2 physisorption results, are given in Table S1.† Keeping in mind the limitations of the BET approximation, we can observe that the parent sample possesses comparable BET and micropore areas as reported in the literature[25,32] and that there are no significant differences in BET surface areas and micropore volumes between the parent and steam-treated samples, except for sample Cu-S750. For all treated catalysts, the pore area is very close to the micropore area, indicating that no mesopores were formed in these samples. This is in line with what we see by XRD, wherein up to 750 °C the crystal structure of the zeolites seems to remain intact, which is something that has been reported before in the literature.[33] For the samples treated with different water contents, there is a general small decrease in BET surface area, micropore volume and micropore area with increasing water content; a summary of this can be found in Table S2.† This shows that part of the

This journal is © The Royal Society of Chemistry 2017

Catal. Sci. Technol., 2017, 7, 3851–3862 | 3855

Table 3 Areas and volumes of the parent and base-leached Cu-SSZ-13 samples, as measured by Ar physisorption

| Sample	[NaOH] (M)	BET (m^2 g^{-1})	External surface area (m^2 g^{-1})	Micropore area (m^2 g^{-1})	Total pore volume (cm^3 g^{-1})	Micropore volume (cm^3 g^{-1})	External pore volume[a] (cm^3 g^{-1})
H-Parent	—	925	25	900	0.37	0.36	0.01
Cu-Parent	—	659	6	653	0.28	0.26	0.02
0.10	0.10	597	17	580	0.24	0.23	0.01
0.15	0.15	402	128	274	0.21	0.10	0.11
0.20	0.2	287	182	105	0.18	0.04	0.14

[a] Total pore volume − *t*-plot micropore volume.

framework has collapsed or became inaccessible due to Cu clustering or framework destruction, but no mesopores were detected using Ar-physisorption, leading us to believe these are not created under these specific steaming conditions.

Pore accessibility as revealed by confocal fluorescence microscopy

Fig. 3 shows the confocal fluorescence microscopy images of various base-leached zeolite Cu-SSZ-13 crystals as well as the parent H-SSZ-13 crystal after staining with DAMPI-1 and DAMPI-4. DAMPI-1 and DAMPI-4 are similar fluorescent probe molecules, but DAMPI-4 has a bigger effective diameter (10.1 Å for DAMPI-4 *vs.* 5.8 Å for DAMPI-1). These fluorescent probe molecules cannot enter the micropores of SSZ-13, which is confirmed by staining the untreated parent H-SSZ-13 (Fig. 3A and E). These crystals show no fluorescence inside the crystal, and only a very small amount at the edge, which is likely caused by probe molecules adsorbed to the crystal

surface. While the probe molecule cannot enter the micropores, it can enter mesopores created by NaOH leaching. The pore size range of the base-leached crystals reaches up to 10 nm (Fig. 2B), and as the probe molecule has only an effective diameter of 5.8 Å to 10.1 Å, it can readily diffuse into the mesopore system. The confined environment causes the probe molecule to become highly fluorescent. Fluorescence observed in the crystal is therefore an indicator for mesoporosity. The base leached mesoporous Cu-SSZ-13 crystals (Fig. 3) show an increasing amount of fluorescent signal. There seems to be an increase in the mesopore volume, as can be seen from the large increase in fluorescence with higher NaOH concentrations. This is likely due to the higher amounts of probe molecules that fit into the larger pore area created by the base leaching. These images also confirm what was already measured using Ar physisorption. For each of the NaOH-leached samples, the distribution of fluorescence is not homogeneous but is rather concentrated at the edge of the crystals. For higher NaOH concentrations, the mesopores
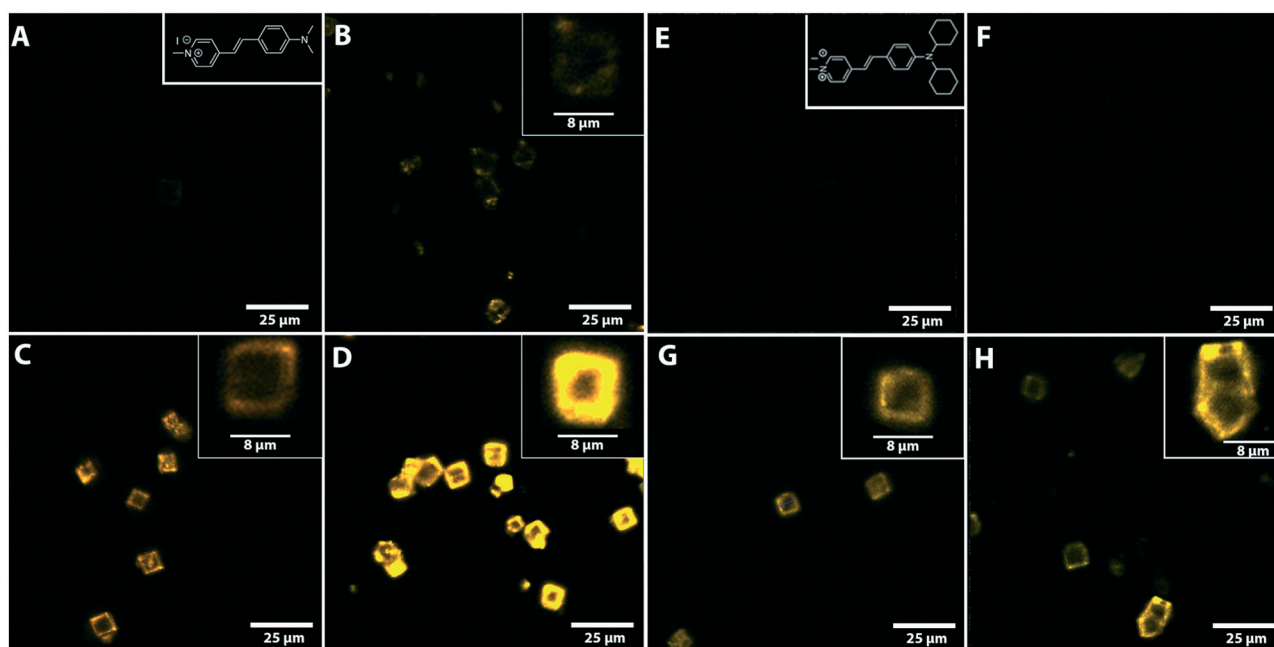
Fig. 3 Confocal fluorescence microscopy images of the parent H-SSZ-13 and the three base-leached zeolite Cu-SSZ-13 crystals under study. Inset in A: DAMPI-1 molecule. The measurements were made in the middle plane of the crystals: A–D using DAMPI-1 probe molecule. A) Parent zeolite H-SSZ-13 crystal; B) zeolite Cu-SSZ-13-0.10; C) Cu-SSZ-13-0.15; D) zeolite Cu-SSZ-13-0.20. E–H using DAMPI-4 probe molecule; inset in E: DAMPI-4 molecule. E) Parent zeolite H-SSZ-13 crystal; F) zeolite Cu-SSZ-13-0.10; G) Cu-SSZ-13-0.15; H) zeolite Cu-SSZ-13-0.20.

3856 | *Catal. Sci. Technol.*, 2017, **7**, 3851–3862

This journal is © The Royal Society of Chemistry 2017

seem to penetrate further into the crystal. However, even for the crystals leached with the highest concentration of NaOH, fluorescence is not observed more than 50% towards the center of the crystal. The middle part of the leached zeolite crystals does not seem to be very accessible to the probes; yet, the fluorescent probes still occupy mostly the spaces in the crust of the zeolite, indicating that the leaching does start from the outside in and does not form mesopores throughout the whole zeolite crystals.

The appearance of fluorescence around the edge of the crystal is also dependent on leaching conditions. In the Cu-SSZ-13-0.10 sample, fluorescence is observed in hotspots around the edges, rather than homogeneously distributed, indicating that once mesopores are formed, the formation of more mesopores in that area is accelerated. For the samples leached with higher NaOH concentrations, fluorescence around the edges appears more homogeneous.

After staining the samples with DAMPI-4 (Fig. 3E and H), we still see a similar trend to the staining with DAMPI-1; the fluorescence increases with increasing base concentration. From the Ar physisorption data, it was already clear that the sample desilicated using 0.1 M NaOH only had pores $\lesssim 2$ nm. After staining with DAMPI-4, almost no fluorescence is visible, confirming that this sample has only very small pores (most of them <1 nm). For the two samples base-leached with higher NaOH concentrations, the fluorescence is clearly visible but of a lower intensity than after staining with DAMPI-1. This also relates nicely with the Ar-physisorption data; higher NaOH concentrations lead to bigger mesopores.

For the steamed samples, the same staining experiments with fluorescent probe molecules were performed as for the parent sample, and the samples were severely steamed at 650 and 750 °C. These samples were selected since the samples steamed at higher temperatures should in theory show formation of more mesopores, if present. These samples were all stained using DAMPI-1 and DAMPI-4, to obtain a similar relationship to that present in the base-leached samples. The fluorescence was first recorded using the exact same settings to make it a fair comparison, but no fluorescence was detected using these settings. Fig. S2† shows the confocal fluorescence microscopy images, and it is immediately clear that these samples contain close to no mesopores, compared to the base leached data set, except for the sample steamed at 750 °C. DAMPI-1 shows a very low amount of fluorescence, but after staining with DAMPI-4 no fluorescence is detected using these settings, showing that all the pores that are present are in the range below 1 nm. In order to make the fluorescence visible, the brightness settings were increased 10-fold (Fig. 4). After this we do see a clear fluorescent image while using DAMPI-1, but for DAMPI-4 the fluorescent signal is barely rising above the noise levels of the detector, again showing that the small amount of mesopores that are created using steaming are very small (<1 nm in diameter). Using base leaching, it is possible to selectively create mesopores, starting from the outside to the inside. With all the different conditions used for steaming SSZ-13, we only managed to
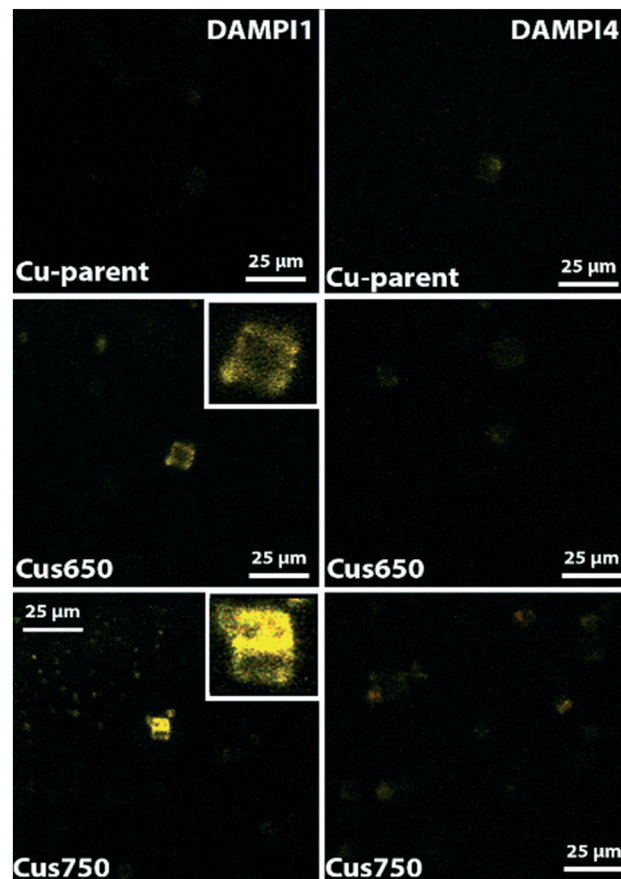

Fig. 4 Confocal fluorescence microscopy images of the parent and two steamed Cu-SSZ-13 zeolite crystals under study. The measurements were made in the middle plane of the crystals. Brightness was increased 10-fold compared to Fig. 3.

create very small mesopores, with an amount so low it could not even be detected using physisorption techniques.

Changes in zeolite acidity upon desilication

To investigate the effect of base leaching on the acid sites and acid strength of the zeolite materials, NH₃-TPD was performed and the results are shown in Fig. 5. Three peaks were observed for the Cu-exchanged zeolites, and two peaks were observed for the H-SSZ-13 zeolite. In previous studies,[23,34,35] acid sites have been characterized in great detail. The low temperature peak (LT) is assigned to weakly absorbed NH₃, such as physisorbed NH₃ and NH₃ adsorbed on weak Lewis acid sites. The intermediate temperature peak (IT) at around 300 °C is assigned to NH₃ adsorbed on strong Lewis acid sites, caused by $e.g.$ the incorporation of Cu^{2+} ions. The high temperature peak (HT) starting from around 380 °C is related to NH₃ adsorbed on Brønsted acid sites. The integrated total acidity amounts are listed in Table 2. A decrease in overall acidity is observed using increasing NaOH concentrations; however, the sample leached at 0.1 M seems to be very similar to the parent sample; so, it is pointing to a very similar chemical environment. Sommer $et\ al.$ reported
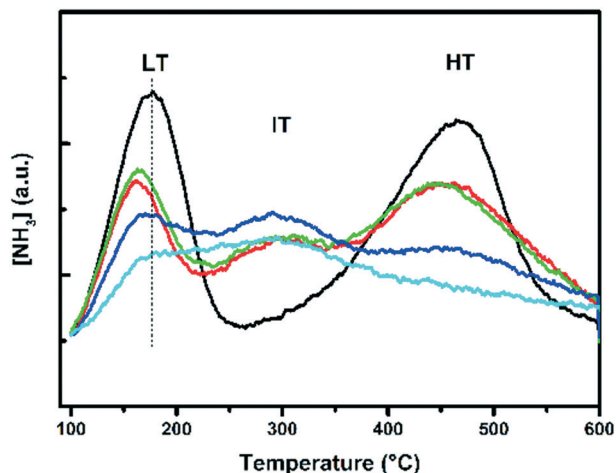
This journal is © The Royal Society of Chemistry 2017

Catal. Sci. Technol., 2017, 7, 3851–3862 | 3857

Fig. 5 NH$_3$-TPD results for the parent and base-leached Cu-SSZ-13 samples. H-parent (black), Cu-parent (red), 0.10 (green), 0.15 (dark blue) and 0.20 (cyan). The 1st peak (LT) is assigned to weakly bound NH$_3$, while the 2nd peak (IT) is due to the interaction of Cu with NH$_3$. The 3rd peak (HT) is assigned to Brønsted acid sites.

that they observed a stronger acid strength for the Lewis acid sites and an unchanged Brønsted acid strength, according to their CO-FT-IR measurements.[25] Our measurements, however, show that there is a decrease in Brønsted acidity, as is evident from Fig. 5, where the peak at 467 °C decreases in intensity, indicating less Brønsted acid sites, and a shift to lower temperatures, indicating weaker Brønsted acid sites. There is, however, an increase in Lewis acid strength if we compare the parent Cu-SSZ-13 sample to the other Cu-SSZ-13 samples. There seems to be less Lewis acidity, but slightly stronger, as indicated by the increase of the peak maximum toward higher temperatures.

Steaming instead of base leaching has a slightly different effect on the SSZ-13 zeolites. Severe steaming treatments remove most Brønsted acid sites (Fig. S3B and D†). After mild steaming at 500 °C, the peak maximum does not shift, indicating a decrease in the amount of Brønsted acid sites, but the steaming treatment preserves the acid strength of these sites at this temperature. This is already different from base leaching, as the mildest base leaching does not significantly alter the acidity of the zeolite. The intermediate temperature (IT) peak is only present in the Cu samples (Fig. S3C–E†), and this is due to the interaction of NH$_3$ with Cu. If we compare Cu-SSZ-13 with H-SSZ-13 (Fig. S3C and D vs. A and B†), it is observed that Cu-SSZ-13 samples desorb more NH$_3$, but this is logical since Cu also interacts with NH$_3$, yielding a higher total integrated NH$_3$ amount, in comparison with samples without Cu (Table S3†). The results presented here show the impact of steaming on the structure of the catalyst, affecting both the zeolite framework and the active Cu^{2+} sites. After severe steaming at 650 °C, no Brønsted acid sites can be seen in the desorption profiles, while in the case of severe steaming at 500 °C the Brønsted acidity is lowered but is still present. The difference between the mild and severe steaming treatment is present and more pronounced for the

H-form of SSZ-13 (Fig. S3A vs. B†). In the case of Cu-SSZ-13, the Brønsted acidity is similar to those of the mild and severe samples treated at the same temperature. Increasing the water content in the feed also causes a gradual decrease in Brønsted acidity. Fig. S3-E† shows the influence of varying water content, which follows the same trend with increasing steam temperature. An increase in aging temperature, time and water content in the feed causes a gradual decrease in the amount of Brønsted acid sites.

Cu coordination state as revealed by UV-vis-NIR diffuse reflectance spectroscopy

To obtain a better understanding of the local coordination and dispersion of the Cu species inside the zeolite framework, the Cu-based catalysts in their hydrated form were analysed using UV-vis-NIR diffuse reflectance spectroscopy (DRS), and the results are given in Fig. 6. Two characteristic absorption bands can generally be found for Cu-exchanged zeolites. The intense transition at ~47 000 cm^{-1} is due to the ligand-to-metal charge transfer of lattice oxygen to Cu^{2+}, while the weaker transition at around 12 000 cm^{-1} is due to the Cu^{2+} d–d transition.[2] The formation of another absorption band at around 40 000 cm^{-1} is generally assigned to Cu$_x$O$_y$ clusters, meaning that some of the Cu^{2+} ions are not in their totally isolated state anymore.[36] Generally speaking, we observe that the intensity of the absorption band at around 40 000 cm^{-1} increases with increasing NaOH concentrations, meaning that there is an increase in the amount of Cu$_x$O$_y$ species. This is something that can be expected, as less exchange sites are present after desilication of the framework due to the decrease in exchangeable surface area, while the ion exchange procedure was kept constant for all the zeolite
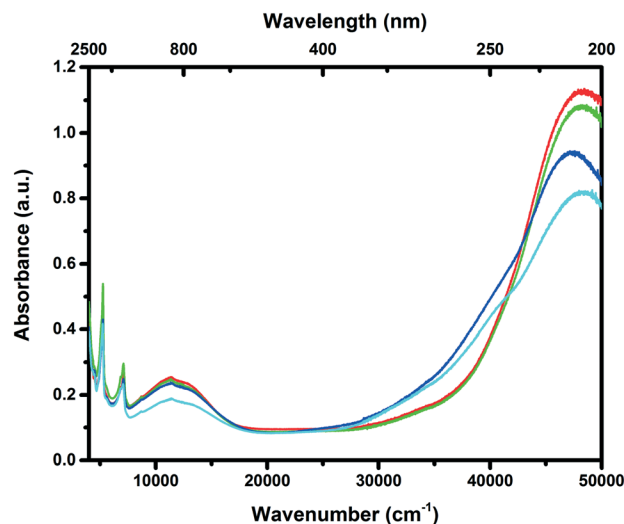

Fig. 6 UV-vis-NIR diffuse reflectance spectroscopy (DRS) data of parent and base-treated samples. Cu-parent (red), 0.10 (green), 0.15 (dark blue) and 0.20 (cyan). Measured in their hydrated form. Cu^{2+} d–d transition at ~12 000 cm^{-1}, Cu^{2+} charge transfer bands at 47 000 cm^{-1} band, while the band at 35 000–40 000 cm^{-1} is assigned to Cu$_x$O$_y$.

samples. Previous studies have shown that these Cu oxides are linked to unselective NH_3 oxidation at high temperatures.[37] For the 0.1 M leached sample, both the acidity and pore surface area/pore volume are very similar to the parent sample, and this results in a close to identical Cu UV-vis-NIR DRS spectrum to the parent sample as well, showing that the chemical environment of the 0.1 M leached sample is similar to that of the parent sample but with an increased accessibility at the surface of the crystals.

Steaming is expected to have a more pronounced effect on the Cu sites inside the zeolite, since steaming removes Al where the Cu anchors, while leaching removes Si, and should in theory have less negative effects. Three main effects of the steaming temperature on the UV-vis-NIR DRS spectra can be observed (Fig. S4†): (I) the Cu^{2+} charge transfer band (~47 000 cm^{-1}) shifts towards lower wavenumbers as the temperature is increased. (II) The adsorption band at ~40 000 cm^{-1} intensifies and broadens, along with a decrease in the Cu^{2+} CT band at 47 000 cm^{-1}. (III) The d–d band at ca. 12 000 cm^{-1} shifts towards higher wave numbers. The band at 40 000 cm^{-1} band is normally attributed to the formation of Cu_xO_y species.[36] These Cu_xO_y species are formed upon the removal of Al from the framework. With less Al, less charge compensation is available, and the Cu^{2+} ions can migrate to form Cu_xO_y clusters. Another possibility is the formation of Cu-aluminate ($CuAl_xO_y$) phases, which has been reported before by Albarracin-Caballero et al.[38] In combination with a noticeable color change (from blue to green or grey), the formation of either Cu_xO_y clusters or $CuAl_xO_y$ phases is well demonstrated. Fig. S4D† shows the reference spectra of bulk CuO and bulk $CuAl_2O_4$. From these reference spectra, it is quite difficult to separate these two different contributions. Also note that bulk CuO has a different UV-vis-NIR DRS spectrum compared to small Cu_xO_y clusters confined in the pores of the zeolite. Both of these phases are not active in the SCR of NO_x, and CuO has been shown to be responsible for NH_3 oxidation.[37] With increasing steam content, more Cu_xO_y or $CuAl_xO_y$ species are formed, as can be seen in Fig. S4C,† demonstrating that increasing the steam content has the same effect as increasing the steaming temperature. The shifting of the Cu^{2+} CT band at 47 000 cm^{-1}, as well as the shifting of the d–d band at 12 000 cm^{-1}, is explained by the changing electron donor strength of the zeolite framework. As Al is removed from the framework as a result of the steaming treatment, the Si/Al ratio changes, introducing a decreased donor strength of the zeolite framework, which results in a shift to lower wavenumbers of the Cu^{2+} CT band.[39,40] Albarracin-Caballero et al.[38] used a higher temperature and a lower water content to deactivate their Cu-SSZ-13 zeolites (800 °C, 10%$_v$ H_2O, to mimic the 135 000 mile road test). They also observed a change in their UV-vis-NIR DRS spectra, i.e. the creation of either Cu oxides or Cu aluminates, but it was not as severe as what we report here. From this, we may conclude that the water content has a large influence on the state of Cu-SSZ-13.

Catalytic performance testing

The NH_3-SCR reaction was performed on the parent Cu-SSZ-13 sample at a GHSV of 100 000 h^{-1} in the temperature region of 150–450 °C, and a comparison was made with the steamed and base-leached samples. The results of this comparison are presented in Fig. 7. Gao et al. have found that pore diffusion limitations play a significant role in the low-temperature kinetics of the Cu-SSZ-13 catalyst.[13] Our parent Cu-SSZ-13 material shows a good NH_3-SCR performance, converting up to 90% of the NO in the temperature window 250–450 °C. It is known that NO conversions drop after 400 °C due to nonselective NH_3 oxidation.[41]

In a first set of experiments, we have compared the parent Cu-SSZ-13 sample with the corresponding steamed samples, and Fig. 7A–C show the effect of the various steaming conditions on NO conversion during the NH_3-SCR reaction. The water content in the feed does not seem to have any effect on the low temperature NO conversions (Fig. 7A). In the high temperature regime, we do however see some effects of the hydrothermal treatment. At 15%$_v$ water content, the sample shows a higher conversion than the parent material; this improvement can be caused by the Cu^{2+} ions migrating to a more ideal ion exchange site, since it is known that H_2O at elevated temperatures can make the Cu^{2+} ion mobile, changing its location.[43] At higher water contents in the feed, however, the high temperature NO conversions decrease, which is something that was expected from the higher amount of Cu oxides or Cu aluminates, as witnessed by UV-vis-NIR DRS. The influence of temperature on NO conversion is slightly different. In the low temperature regime, we do observe a decrease in NO conversions during the NH_3-SCR reaction. Samples that were hydrothermally deactivated at temperatures lower than 750 °C only lose a small amount of their NH_3-SCR activity, while substantial catalyst deactivation is seen after severe hydrothermal deactivation at 750 °C (Fig. 7C).

In a second series of experiments, we have made a comparison between the parent, steamed and base-leached Cu-SSZ-13 materials, and the results are summarized in Fig. 7D. The samples base leached at 0.1 M show an increase in both activity and N_2 selectivity during the NH_3-SCR reaction, reaching close to 100% conversion between 250 and 400 °C. The low temperature catalytic activity and selectivity for this catalyst material is also greatly increased, showing that the introduction of the right amount of mesopores can greatly enhance the low temperature performance of the Cu-SSZ-13 NH_3-SCR catalyst. This is important since new diesel engines lead to a lower exhaust temperature than those of the older diesel engines.[42] There does, however, seem to be an optimum in NaOH concentration, since higher concentrations of NaOH lower the catalytic activity of the Cu-SSZ-13 zeolites – even lower than that of the parent material (below 90% conversion). At 450 °C, however, the 0.15 M leached sample still outperforms the parent Cu-SSZ-13 catalyst, which is probably due to the better accessibility. The 0.20 M leached catalyst material shows a very significant decrease over the whole
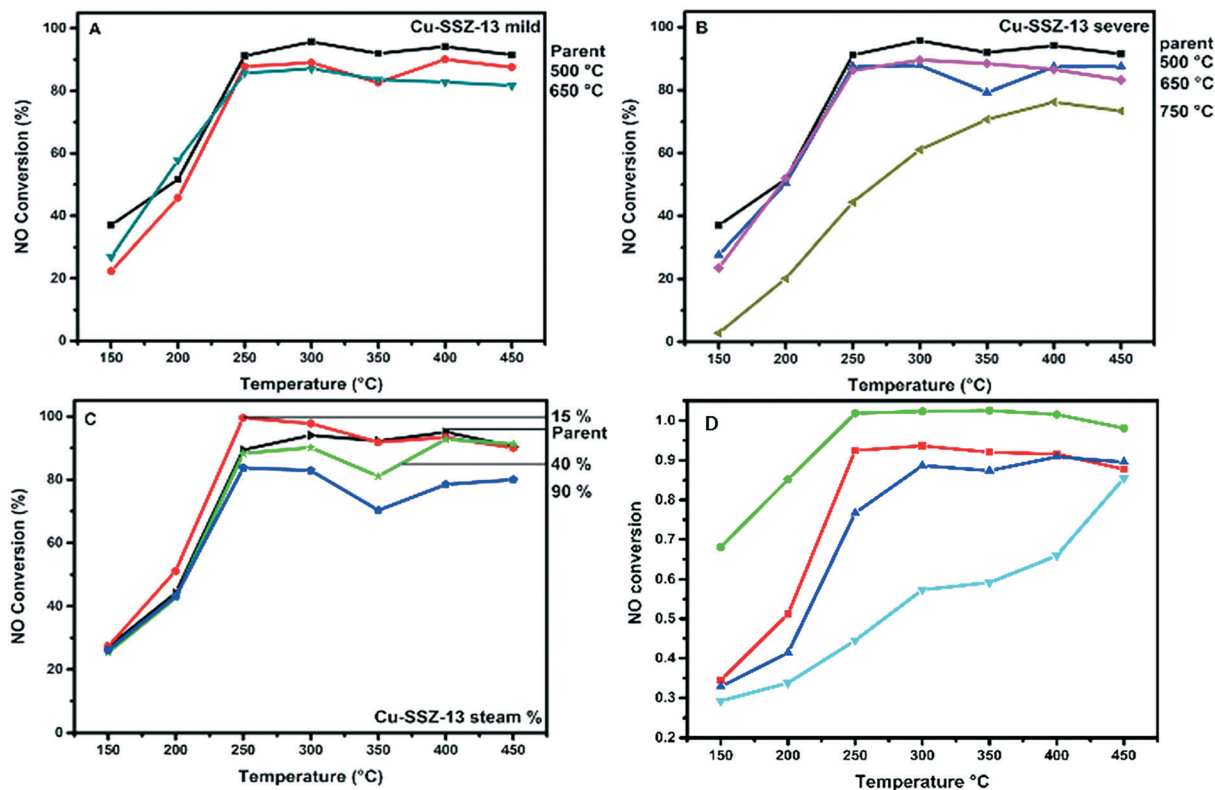
This journal is © The Royal Society of Chemistry 2017

Catal. Sci. Technol., 2017, 7, 3851–3862 | 3859

Fig. 7 NO conversions of parent and steamed Cu-SSZ-13 samples using differing steam treatments: A) mild steaming treatments, B) severe steaming treatments, C) influence of water content in the feed, D) influence of base leaching. Cu-parent (red), 0.10 (green), 0.15 (dark blue) and 0.20 (cyan) during the NH_3-SCR in steady state mode (GHSV = 100 000 h^{-1}).

measured temperature window but still comes close to the catalytic performance of the parent sample at 450 °C.

From the calculations we performed on the catalyst, by making use of the paper by Gao *et al.*,[13] we estimate that the effectiveness factor of our catalyst is only 0.05, at temperatures below 200 °C. This would mean only 5% of the catalyst is being used at these reaction temperatures. Introducing larger mesopores only in the outer crust of zeolite crystals would therefore greatly enhance the catalytic performance, since the low temperature regime is dominated by intra-particle diffusion limitation.[13] However, although both the 0.15 and 0.2 M leached Cu-SSZ-13 samples have higher accessibilities compared to the parent and 0.1 M leached samples, they show a decreased NO_x conversion and selectivity with respect to the parent Cu-SSZ-13 catalyst. This leads to some important insights about how the catalyst should be synthesized. As has been discussed, the NH_3-TPD shows that less acid sites are present in these samples, in comparison with the parent and 0.1 M leached Cu-SSZ-13 samples. It seems that the chemical environment also plays a role in optimizing the catalyst material. If one introduces more accessibility, one should try to keep the acidity and chemical environment inside the zeolite very similar, as is also the case for the 0.1 M leached Cu-SSZ-13 catalyst in comparison with the parent Cu-SSZ-13.

The observations made in Fig. 7 are very interesting in view of the data obtained by the different characterization

techniques, such as the UV-vis-NIR DRS and NH_3-TPD measurements. Indeed, they show major changes at these lower deactivation temperatures for the steamed samples, including the Cu_xO_y cluster, $CuAl_xO_y$ phase formation and the removal of Brønsted acidity, but this does not seem to significantly impact the catalytic performances of these materials. The sample steamed at 750 °C also shows framework degradation, which might cause the severe drop in NH_3-SCR activity. For all the other steaming conditions, some of the Cu species cluster to Cu_xO_y- or $CuAl_xO_y$-like species and most of the Brønsted acidity is removed (based on NH_3-TPD results), but this has only a limited negative effect on NH_3-SCR activity, showing how remarkably stable the Cu-SSZ-13 system really is under steaming conditions, in comparison with medium and large pore zeolites. One remark that should be made here is that our zeolite materials have a high Cu-exchange ratio, and it is known that the higher the Cu content in the zeolite, the weaker the hydrothermal stability will be.[28] This might explain why Cu is not protecting the zeolite, as has also been suggested for low Cu loadings, but is actually destroying the zeolite.[28] Earlier research papers have already shown that Brønsted acidity is not a real necessity for having a very active NH_3-SCR catalyst.[44] This was demonstrated by using Na or other alkaline metal ions to remove Brønsted acidity. In our case, the Brønsted acidity was removed by steaming, but no other chemical species were introduced into the zeolite material. Removal of Brønsted acid

3860 | *Catal. Sci. Technol.*, 2017, **7**, 3851–3862

This journal is © The Royal Society of Chemistry 2017

sites, or clustering of some of the Cu species, seems to have little impact on the catalysis of the Cu-zeolites under study, as far as we observed. Based on the research of Di Iorio *et al.* (Si/Al = 4.5 Cu/Al = 0–0.2),[45] we feel we have to mention that Cu^{2+} connected to 2 framework oxygen atoms (so two aluminium atoms close by) will react with NH_3 under reaction conditions to form Cu^+ and a H^+ site on the other framework oxygen, which can in turn form NH_4^+, which is believed to be one of the intermediate steps in the NH_3-SCR. Structural collapse, however, is the main route of deactivation for Cu-SSZ-13 catalysts. Furthermore, Cu seems to destabilize the Cu-SSZ-13 framework with respect to H-SSZ-13, as there is greater structural collapse in the severely treated Cu samples (as witnessed from the XRD measurements).

By comparing the introduction of mesopores *via* steaming with that *via* base leaching, we show that base leaching creates a more active catalyst in the low temperature regime, if the right conditions are used. For all the steaming treatments we performed, we never managed to outperform the parent zeolite catalyst and only witnessed deactivation.

Conclusions

Mesopores with diameters of 2–10 nm were introduced into zeolite H-SSZ-13 after alkaline treatment using NaOH. The alkaline treatment causes desilication of the framework structure resulting in an improved accessibility of the zeolite framework. Subsequently, Cu was loaded on these mesoporous zeolite materials and it was found that the Cu-catalyst treated with 0.1 M NaOH showed an improved performance for the NH_3-SCR reaction. More specifically, this catalyst allows the improvement of both the low and the high temperature catalytic performance, increasing the NO conversion in the temperature range of 250–450 °C from ~90% for the parent material to ~100% for the 0.1 M NaOH sample. In particular, the improved low temperature performance (*i.e.*, a two-fold increase at 150 and 250 °C) of these mesoporous Cu-SSZ-13 catalysts is of great interest. It was found that the chemical environment of Cu-SSZ-13-0.1 was very similar to that of the parent sample but had a slightly increased accessibility at the surface. Only a small part of the zeolite crystal is being used at these low reaction temperatures, due to intra-particle diffusion limitation. Creating mesopores limited to the surface while keeping the overall zeolite crystal intact therefore makes an improved NH_3-SCR catalyst. On the other hand, higher concentrations of NaOH reduce the catalytic activity of the Cu-SSZ-13 zeolites – even lower than that of the parent material – by decreasing the accessible surface area and acidity. At 450 °C, however, the 0.15 M leached sample outperforms the parent Cu-SSZ-13 catalyst while showing lower conversions over the whole temperature range. The 0.2 M leached sample performs worse but shows similar conversions to the parent Cu-SSZ-13 sample at 450 °C. The development of these mesopores was accompanied by a loss of total surface area and at higher concentrations a loss in overall crystallinity. Based on the NH_3-TPD measurements, both the Lewis and Brønsted acid sites decreased in amount, while the Lewis acid sites became slightly stronger, and the Brønsted acid sites became a little weaker with increasing base concentrations. Confocal fluorescence microscopy showed that the mesopores are formed mostly on the outside of the zeolite SSZ-13 crystals and slowly move more towards the inner core of the zeolite SSZ-13 crystals with increasing amount of NaOH – a finding which was also confirmed with SEM measurements. For comparison, we also investigated the effects of hydrothermal aging temperature, duration and water content on the catalytic performance and stability of both H-SSZ-13 and Cu-SSZ-13 for the selective catalytic reduction (SCR) of NO with NH_3. Fresh Cu-SSZ-13 shows excellent catalytic activity, and only after severely treating the sample at 750 °C was a major drop in activity over the whole temperature region observed. This was attributed to severe dealumination, leading to zeolite framework collapse. For all other steaming conditions (*i.e.*, 500 and 650 °C) and a water content of 80%, some of the Cu species cluster to either Cu_xO_y- or $CuAl_yO_x$-like species, while most of the Brønsted acidity is removed, but this has only a limited negative effect on NH_3-SCR activity, showing the remarkable stability of the Cu-SSZ-13 system in comparison with, for example, Cu-BEA or Cu-MFI. Steaming the samples, however, never improved the catalyst as base leaching managed to; it always deactivated the catalyst slightly. Possible reasons are that steaming is not effective in creating mesopores, and that mesopores seem to have a positive effect in the low temperature NH_3-SCR region. Furthermore, steaming zeolites produces way more Cu_xO_y clusters or $CuAl_xO_y$ phases, due to the removal of ion-exchange sites, while the acidity and chemical nature of the zeolite is more altered in the case of steaming, as opposed to base leaching zeolites using low NaOH concentrations.

Acknowledgements

References

1 S. Brandenberger, O. Kröcher, A. Tissler and R. Althoff, *Catal. Rev.: Sci. Eng.*, 2008, **50**, 492–531.

2 S. T. Korhonen, D. W. Fickel, R. F. Lobo, B. M. Weckhuysen and A. M. Beale, *Chem. Commun.*, 2011, **47**, 800–802.

3 U. Deka, I. Lezcano-González, S. J. Warrender, A. Lorena Picone, P. A. Wright, B. M. Weckhuysen and A. M. Beale, *Microporous Mesoporous Mater.*, 2012, **166**, 144–152.

4 U. Deka, A. Juhin, E. A. Eilertsen, H. Emerich, M. A. Green, S. T. Korhonen, B. M. Weckhuysen and A. M. Beale, *J. Phys. Chem. C*, 2012, **116**, 4809–4818.

This journal is © The Royal Society of Chemistry 2017

Catal. Sci. Technol., 2017, **7**, 3851–3862 | 3861

5   I. Lezcano-González, U. Deka, H. E. van der Bij, P. Paalanen, B. Arstad, B. M. Weckhuysen and A. M. Beale, *Appl. Catal., B*, 2014, **154–155**, 339–349.

6   D. W. Fickel, E. D'Addio, J. A. Lauterbach and R. F. Lobo, *Appl. Catal., B*, 2011, **102**, 441–448.

7   J. H. Kwak, R. G. Tonkyn, D. H. Kim, J. Szanyi and C. H. F. Peden, *J. Catal.*, 2010, **275**, 187–190.

8   A. M. Beale, F. Gao, I. Lezcano-González, C. H. F. Peden and J. Szanyi, *Chem. Soc. Rev.*, 2015, **44**, 7371–7405.

9   H. Chen, I. Nova, E. Tronconi, H. Chen, I. Nova and E. Tronconi, *Urea-SCR Technology for deNOx After Treatment of Diesel Exhausts*, Springer, New York, 2014.

10 R. Oord and B. M. Weckhuysen, in *Zeolites and Zeolite-Like Materials*, ed. B. F. Sels and L. M. Kustov, Elsevier, Amsterdam, 2016, pp. 433–450.

11 J. H. Kwak, D. Tran, S. D. Burton, J. Szanyi, J. H. Lee and C. H. F. Peden, *J. Catal.*, 2012, **287**, 203–209.

12 Y. Tao, H. Kanoh, L. Abrams and K. Kaneko, *Chem. Rev.*, 2006, **106**, 896–910.

13 F. Gao, E. D. Walter, E. M. Karp, J. Luo, R. G. Tonkyn, J. H. Kwak, J. Szanyi and C. H. F. Peden, *J. Catal.*, 2013, **300**, 20–29.

14 F. Giordanino, P. N. R. Vennestrøm, L. F. Lundegaard, F. N. Stappen, S. Mossin, P. Beato, S. Bordiga and C. Lamberti, *Dalton Trans.*, 2013, **42**, 12741–12761.

15 E. Borfecchia, K. A. Lomachenko, F. Giordanino, H. Falsig, P. Beato, A. V. Soldatov, S. Bordiga and C. Lamberti, *Chem. Sci.*, 2014, **6**, 548–563.

16 T. V. W. W. Janssens, H. Falsig, L. F. Lundegaard, P. N. R. Vennestrøm, S. B. Rasmussen, P. G. Moses, F. Giordanino, E. Borfecchia, K. A. Lomachenko, C. Lamberti, S. Bordiga, A. Godiksen, S. Mossin and P. Beato, *ACS Catal.*, 2015, **5**, 2832–2845.

17 K. A. Lomachenko, E. Borfecchia, C. Negri, G. Berlier, C. Lamberti, P. Beato, H. Falsig and S. Bordiga, *J. Am. Chem. Soc.*, 2016, **138**, 12025–12028.

18 C. Tyrsted, E. Borfecchia, G. Berlier, K. A. Lomachenko, C. Lamberti, S. Bordiga, P. N. R. Vennestrøm, T. V. W. Janssens, H. Falsig, P. Beato and A. Puig-Molina, *Catal. Sci. Technol.*, 2016, **6**, 8314–8324.

19 C. Paolucci, A. A. Parekh, I. Khurana, J. R. Di Iorio, H. Li, J. D. Albarracin Caballero, A. J. Shih, T. Anggara, W. N. Delgass, J. T. Miller, F. H. Ribeiro, R. Gounder and W. F. Schneider, *J. Am. Chem. Soc.*, 2016, **138**, 6028–6048.

20 S. A. Bates, A. A. Verma, C. Paolucci, A. A. Parekh, T. Anggara, A. Yezerets, W. F. Schneider, J. T. Miller, W. N. Delgass and F. H. Ribeiro, *J. Catal.*, 2014, **312**, 87–97.

21 C. Paolucci, A. A. Verma, S. A. Bates, V. F. Kispersky, J. T. Miller, R. Gounder, W. N. Delgass, F. H. Ribeiro and W. F. Schneider, *Angew. Chem., Int. Ed.*, 2014, **53**, 11828–11833.

22 M. Y. Kustova, S. B. Rasmussen, A. L. Kustov and C. H. Christensen, *Appl. Catal., B*, 2006, **67**, 60–67.

23 T. Zhang, F. Qiu and J. Li, *Appl. Catal., B*, 2016, **195**, 48–58.

24 A. L. Kustov, T. W. Hansen, M. Kustova and C. H. Christensen, *Appl. Catal., B*, 2007, **76**, 311–319.

25 L. Sommer, D. Mores, S. Svelle, M. Stöcker, B. M. Weckhuysen and U. Olsbye, *Microporous Mesoporous Mater.*, 2010, **132**, 384–394.

26 A. M. Beale, I. Lezcano-Gonzalez, W. A. Slawinksi and D. S. Wragg, *Chem. Commun.*, 2016, **52**, 6170–6173.

27 F. C. Hendriks, D. Valencia, P. C. A. Bruijnincx and B. M. Weckhuysen, *Phys. Chem. Chem. Phys.*, 2017, **19**, 1857–1867.

28 M. Moliner, C. Franch, E. Palomares, M. Grill and A. Corma, *Chem. Commun.*, 2012, **48**, 8264–8266.

29 C. Seebacher, J. Rau, F.-W. Deeg, C. Bräuchle, S. Altmaier, R. Jäger and P. Behrens, *Adv. Mater.*, 2001, **13**, 1374–1377.

30 M. B. J. Roeffaers, R. Ameloot, M. Baruah, H. Uji-i, M. Bulut, G. De Cremer, U. Müller, P. A. Jacobs, J. Hofkens, B. F. Sels and D. E. De Vos, *J. Am. Chem. Soc.*, 2008, **130**, 5763–5772.

31 F. C. Hendriks, J. E. Schmidt, J. A. Rombouts, K. Lammertsma, C. A. Pieter and B. M. Weckhuysen, *Chem. – Eur. J.*, 2017, **23**, 6305–6314.

32 L. Wu, V. Degirmenci, P. C. M. M. Magusin, N. J. H. G. M. Lousberg and E. J. M. Hensen, *J. Catal.*, 2013, **298**, 27–40.

33 Y. J. Kim, J. K. Lee, K. M. Min, S. B. Hong, I.-S. Nam and B. K. Cho, *J. Catal.*, 2014, **311**, 447–457.

34 D. Wang, F. Gao, C. H. F. Peden, J. Li, K. Kamasamudram and W. S. Epling, *ChemCatChem*, 2014, **6**, 1579–1583.

35 F. Gao, N. M. Washton, Y. Wang, M. Kollár, J. Szanyi and C. H. F. Peden, *J. Catal.*, 2015, **331**, 25–38.

36 A. El-Trass, H. ElShamy, I. El-Mehasseb and M. El-Kemary, *Appl. Surf. Sci.*, 2012, **258**, 2997–3001.

37 D. Wang, L. Zhang, J. Li, K. Kamasamudram and W. S. Epling, *Catal. Today*, 2013, **231**, 64–74.

38 J. D. Albarracin-Caballero, I. Khurana, J. R. Di Iorio, A. J. Shih, J. E. Schmidt, M. Dusselier, M. E. Davis, A. Yezerets, J. T. Miller, F. H. Ribeiro and R. Gounder, *React. Chem. Eng.*, 2017, 7–10.

39 S. Y. Choi, Y. S. Park, S. B. Hong and K. B. Yoon, *J. Am. Chem. Soc.*, 1996, **118**, 9377–9386.

40 S. A. Yashnik, A. V. Salnikov, N. T. Vasenin, V. F. Anufrienko and Z. R. Ismagilov, *Catal. Today*, 2012, **197**, 214–227.

41 I. Lezcano-González, U. Deka, B. Arstad, A. Van Yperen-De Deyne, K. Hemelsoet, M. Waroquier, V. Van Speybroeck, B. M. Weckhuysen and A. M. Beale, *Phys. Chem. Chem. Phys.*, 2014, **16**, 1639–1650.

42 M. Zammit, C. Dimaggio, C. Kim, C. Lambert, G. Muntean, C. Peden, J. Parks and K. Howden, *Future Automotive After Treatment Solutions : The 150 °C Challenge Workshop Report*, 2012.

43 W. Su, Z. Li, Y. Peng and J. Li, *Phys. Chem. Chem. Phys.*, 2015, **17**, 29142–29149.

44 F. Gao, Y. Wang, N. M. Washton, M. Kollár, J. Szanyi and C. H. F. Peden, *ACS Catal.*, 2015, **5**, 6780–6791.

45 J. R. Di Iorio, S. A. Bates, A. A. Verma, W. N. Delgass, F. H. Ribeiro, J. T. Miller and R. Gounder, *Top. Catal.*, 2015, **58**, 424–434.